Asymmetric Thermal Relaxation in Driven Systems: Rotations go Opposite Ways

Cai Dieball,[1] Gerrit Wellecke,[1, 2] and Aljaž Godec[1, *]

[1]*Mathematical bioPhysics group, Max Planck Institute for Multidisciplinary Sciences, Göttingen 37077, Germany*
[2]*Present address: Theory of Biological Fluids, Max Planck Institute*
for Dynamics and Self-Organization, Göttingen 37077, Germany

It was predicted and recently experimentally confirmed that systems with microscopically reversible dynamics in locally quadratic potentials warm up faster than they cool down. This thermal relaxation asymmetry challenged the local-equilibrium paradigm valid near equilibrium. Because the intuition and proof hinged on the dynamics obeying detailed balance, it was not clear whether the asymmetry persists in systems with irreversible dynamics. To fill this gap, we here prove the relaxation asymmetry for systems driven out of equilibrium by a general linear drift. The asymmetry persists due to a non-trivial isomorphism between driven and reversible processes. Moreover, rotational motions emerge that, strikingly, occur in opposite directions during heating and cooling. This highlights that noisy systems do *not* relax by passing through local equilibria.

According to the laws of thermodynamics, systems in contact with a thermal environment evolve to the temperature of their surroundings in the process called *thermal relaxation* [1]. Relaxation close to equilibrium may be explained by linear response theory conceptually based on Onsager's regression hypothesis [2–4]. That is, relaxation from a temperature quench is indistinguishable from the decay of a spontaneous thermal fluctuation at equilibrium [2–4]. Analogous results were meanwhile formulated also for relaxation near non-equilibrium steady states [5–7]. Beyond the linear regime, however, the regression hypothesis and perturbative arguments fail.

Important advances have been made in understanding relaxation beyond the linear regime addressing hydrodynamic limits [8, 9], barrier crossing in driven systems [10, 11], memory effects [12–21], far-from-equilibrium fluctuation-dissipation theorems [22, 23], optimal heating/cooling protocols [24], anomalous relaxation also known as the *Mpemba effect* [25–32] and its isothermal analogue [33], the Kovacs effect [34, 35], and dynamical phase transitions [36–44]. Important advances further include transient thermodynamic uncertainty relations [45–50], speed limits [51–55], and analyses of relaxation from the viewpoint of information geometry [54–56].

A particularly striking feature of relaxation was unraveled with the discovery of the asymmetry between heating and cooling from thermodynamically equidistant temperature quenches [57]. That is, it was found that systems with locally quadratic energy landscapes and microscopically reversible dynamics heat up faster than they cool down. Later works expanded on this result [58–60]. The asymmetry was recently quantitatively confirmed by experiments [56].

The asymmetry emerges because the entropy production within the system during heating is more efficient than heat dissipation into the environment during cooling [57]. In turn, close to equilibrium they become equivalent and symmetry is restored [56, 57]. An even deeper understanding of the asymmetry was recently achieved by means of "thermal kinematics" [56]. However, both the reasoning and the proof of the asymmetry [56, 57, 61] seem to hinge on the reversibility of the dynamics. Therefore, the persistence of the asymmetry in systems driven into non-equilibrium steady states (NESS) was unexpected. In particular, a non-conservative force profoundly changes relaxation behavior [62–65] even near stable fixed points [66] and in systems with linear drift [67], and may thus *a priori* also break the asymmetry.
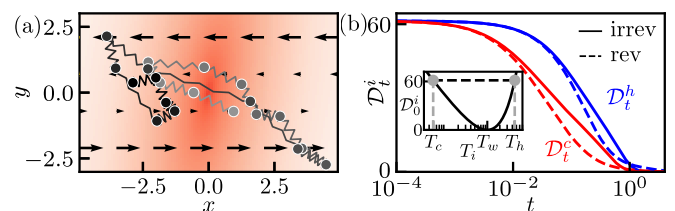
FIG. 1. (a) Configuration of a harmonically confined (color gradient) Rouse polymer with $N = 20$ beads in 3d with hydrodynamic interactions and internal friction subject to a shear flow (arrows) in the x-y-plane drawn from the NESS with covariance $\mathbf{\Sigma}_{s,w}$ (see [68] for parameters); a projection onto the x-y-plane is shown. (b) The corresponding free energy difference $\mathcal{D}_t^i$ in Eq. (5) during heating from T_c (red) and cooling from T_h (blue) with (solid lines) and without (dashed lines) irreversible shear flow. The shear changes $\mathcal{D}_t^i$, but the thermal relaxation asymmetry $\mathcal{D}_t^c < \mathcal{D}_t^h$ for $t > 0$ remains valid. Inset: Temperatures T_i before the quench are chosen thermodynamically equidistant, i.e. $\mathcal{D}_0^c = \mathcal{D}_0^h$.

Here, we investigate the speed and asymmetry of thermal relaxation to an NESS. As a paradigmatic example we first consider a harmonically confined Rouse polymer with hydrodynamic interactions and internal friction driven by shear flow (see Fig. 1), and demonstrate that heating is faster than cooling. Next we provide a systematic analysis of relaxation under broken detailed balance and explain under which conditions heating and cooling both become faster. Finally, we prove that *all* ergodic systems with a linear drift, including those driven arbitrarily far from equilibrium and displaying rotational motions,

heat up faster than they cool down. In this regime the notion of a local effective non-equilibrium temperature is *nominally* impossible. Our proof, which exploits dual-reversal symmetry, unravels a non-trivial isomorphism between reversible and driven systems. Finally, we find a new unexpected facet of the relaxation asymmetry—rotational motions occur in *opposite directions* during heating and cooling, respectively.

Setup and motivating example.—The relaxation asymmetry was originally proven for reversible diffusions in locally quadratic energy landscapes as well as their low-dimensional projections [57, 61]. It states that such systems, when quenched from thermodynamically equidistant (TED) temperatures T_h, T_c to an ambient temperature T_w with $T_c < T_w < T_h$, heat up faster than they cool down. In quantitative terms, the generalized excess free energy in units of $k_B T_w$ [66, 69–71] or non-adiabatic entropy production [72, 73] (i.e. the relative entropy in units of k_B [74] between the instantaneous $P_i^w(\mathbf{x}, t)$ and stationary $p_s^w(\mathbf{x})$ probability density at T_w with $i = h, c$)

$$\mathcal{D}_t^i \equiv \mathcal{D}_{\mathrm{KL}}[P_i^w(\mathbf{x},t)||p_s^w(\mathbf{x})] \equiv \int d\mathbf{x} P_i^w(\mathbf{x},t) \ln \frac{P_i^w(\mathbf{x},t)}{p_s^w(\mathbf{x})}, \quad (1)$$

is always smaller during heating [57, 61]. That is, $\mathcal{D}_t^c < \mathcal{D}_t^h$ for all $t > 0$ and all TED T_h and T_c.

In a strict sense, the asymmetry is to be understood as a statement about linearized drift around a local minimum in some high-dimensional energy landscape [57]; counterexamples for diffusion in rugged landscapes [57] and for small quenches also in sufficiently anharmonic wells [60] are known. The generalization to driven systems therefore involves a linear drift that, however, does not derive from a potential and breaks detailed balance. Our main result is the discovery and proof (see last section) of the asymmetry $\mathcal{D}_t^c < \mathcal{D}_t^h$ in driven systems.

Consider a d-dimensional system evolving according to the overdamped Langevin equation [75, 76]

$$d\mathbf{x}_t = -\mathbf{A}\mathbf{x}_t dt + \boldsymbol{\sigma}_i d\mathbf{W}_t, \quad (2)$$

with square drift and noise-amplitude matrices, $\mathbf{A}$ and $\boldsymbol{\sigma}_i$, respectively. In terms of the friction matrix $\boldsymbol{\gamma}$, given by Stokes' law, the positive definite diffusion matrix reads $\mathbf{D}_i \equiv \boldsymbol{\sigma}_i \boldsymbol{\sigma}_i^T / 2 = k_B T_i \boldsymbol{\gamma}^{-1}$ and thus depends linearly on temperature T_i. The external force $\mathbf{F}(\mathbf{x})$ yields a T_i-independent drift $-\mathbf{A}\mathbf{x} = \boldsymbol{\gamma}^{-1}\mathbf{F}(\mathbf{x})$, where $\mathbf{A}$ is generally non-symmetric but confining, i.e. the eigenvalues of $\mathbf{A}$ have positive real parts. Thus, $\mathbf{x}_t$ is ergodic but irreversible with zero-mean Gaussian NESS density $p_s^i(\mathbf{x}) = (2\pi)^{-d/2} \det[\boldsymbol{\Sigma}_{s,i}]^{-1/2} \exp[-\mathbf{x}^T \boldsymbol{\Sigma}_{s,i}^{-1} \mathbf{x}/2]$ where the covariance $\boldsymbol{\Sigma}_{s,i}$ obeys the Lyapunov equation [68]

$$\mathbf{A}\boldsymbol{\Sigma}_{s,i} + \boldsymbol{\Sigma}_{s,i}\mathbf{A}^T = 2\mathbf{D}_i = 2k_B T_i \boldsymbol{\gamma}^{-1}, \quad (3)$$

and thus depends linearly on the temperature T_i. Eq. (3) implies for all T_i the decomposition into reversible $-\mathbf{A}_{\mathrm{rev}}\mathbf{x} \equiv \mathbf{D}_i \nabla \ln p_s^i(\mathbf{x}) = -\mathbf{D}_i \boldsymbol{\Sigma}_{s,i}^{-1}\mathbf{x}$ and irreversible $-\mathbf{A}_{\mathrm{irr}}\mathbf{x} \equiv (-\mathbf{A} + \mathbf{A}_{\mathrm{rev}})\mathbf{x} = -\boldsymbol{\alpha}_i \boldsymbol{\Sigma}_{s,i}^{-1}\mathbf{x}$ drift [77], where $\boldsymbol{\alpha}_i^T = -\boldsymbol{\alpha}_i$ is an antisymmetric matrix [78].

We focus on temperature quenches—instantaneous changes of the environmental temperature at fixed drift. The thermodynamics of relaxation upon a quench $T_i \to T_w$ is fully specified by $\mathcal{D}_t^i$, as the adiabatic entropy production (housekeeping heat divided by T_w) [73] merely embodies the cost of maintaining the NESS [79] and thus need not be considered. Therefore, TED temperatures $T_{h,c}$ correspond to $\mathcal{D}_0^h = \mathcal{D}_0^c$ and are equal to those of a reversible system at the same T_w [57].

Since the initial condition is a zero-mean Gaussian with $\boldsymbol{\Sigma}_i^w(0) = \boldsymbol{\Sigma}_{s,i}$, the probability density is Gaussian for all times with $\boldsymbol{\Sigma}_i^w(t) \equiv \langle \mathbf{x}_t \mathbf{x}_t^T \rangle_i^w - \langle \mathbf{x}_t \rangle_i^w \langle \mathbf{x}_t^T \rangle_i^w$ given by [68]

$$\frac{d}{dt}\boldsymbol{\Sigma}_i^w(t) = -\mathbf{A}\boldsymbol{\Sigma}_i^w(t) - \boldsymbol{\Sigma}_i^w(t)\mathbf{A}^T + 2\mathbf{D}_w$$

$$\Rightarrow \boldsymbol{\Sigma}_i^w(t) = \boldsymbol{\Sigma}_{s,w} + e^{-\mathbf{A}t}[\boldsymbol{\Sigma}_{s,i} - \boldsymbol{\Sigma}_{s,w}] e^{-\mathbf{A}^T t}, \quad (4)$$

where $\langle \cdot \rangle_i^w$ denotes the average over all paths $\mathbf{x}_t$ at temperature T_w evolving from $p_s^i(\mathbf{x})$. Note that $\boldsymbol{\Sigma}_{s,i} = T_i \boldsymbol{\Sigma}_{s,w}/T_w$ [see Eq. (3)]. Introducing $\delta\tilde{T}_i \equiv T_i/T_w - 1$, the generalized excess free energy reads (see [68])

$$\mathcal{D}_t^i = \frac{1}{2}\delta\tilde{T}_i \operatorname{tr}\mathbf{X}(t) - \frac{1}{2}\ln\det\left[\mathbb{1} + \delta\tilde{T}_i \mathbf{X}(t)\right], \quad (5)$$

where we introduced the $d \times d$ matrix

$$\mathbf{X}(t) \equiv e^{-\mathbf{A}t}\boldsymbol{\Sigma}_{s,w}e^{-\mathbf{A}^T t}\boldsymbol{\Sigma}_{s,w}^{-1}, \quad (6)$$

which via Eq. (5) fully describes relaxation dynamics.

As a paradigmatic example for such processes we consider a harmonically confined Rouse polymer with N beads experiencing hydrodynamic interactions [80, 81] and internal friction [82–85] subject to a shear flow, which was investigated experimentally in [86–94]. For a representative configuration of the NESS ensemble, see Fig. 1a. One may also consider colloidal particles in the presence of non-conservative optical forces [95]. The effect of these forces is included in the $3N \times 3N$ drift matrix $\mathbf{A}$ and $3N \times 3N$ noise amplitude $\boldsymbol{\sigma}_i$ [68]. Evaluating $\mathcal{D}_t^i$ for the heating and cooling processes upon quenches from TED temperatures T_h and T_c we find $\mathcal{D}_t^c < \mathcal{D}_t^h$ for all $t > 0$. That is, heating is faster than cooling (the red line in Fig. 1b is at all times below the blue line). This agrees with the relaxation asymmetry predicted [57] and experimentally verified [56] in reversible systems, and provokes the question if this holds for any linear driving.

Systematics of breaking detailed balance.—We now systematically assess the influence of non-equilibrium drifts on relaxation upon a temperature quench. As shown above, *any* linear drift $\mathbf{A}$ for $i = c, w, h$ decomposes as

$$\mathbf{A} = (\mathbf{D}_i + \boldsymbol{\alpha}_i)\boldsymbol{\Sigma}_{s,i}^{-1} \quad \text{with} \quad \boldsymbol{\alpha}_i^T = -\boldsymbol{\alpha}_i. \quad (7)$$

Thus, by choosing any antisymmetric matrix $\boldsymbol{\alpha}_i$ we alter the NESS current as well as $\mathbf{X}(t)$, but neither $\boldsymbol{\Sigma}_{s,i}$ nor $p_s(\mathbf{x})$. We can thus directly compare an NESS with the corresponding reversible system $\boldsymbol{\alpha}_i = \mathbf{0}$ with the same steady state. Note that such a direct comparison is *not* given in the example in Fig. 1, since the shear flow alters
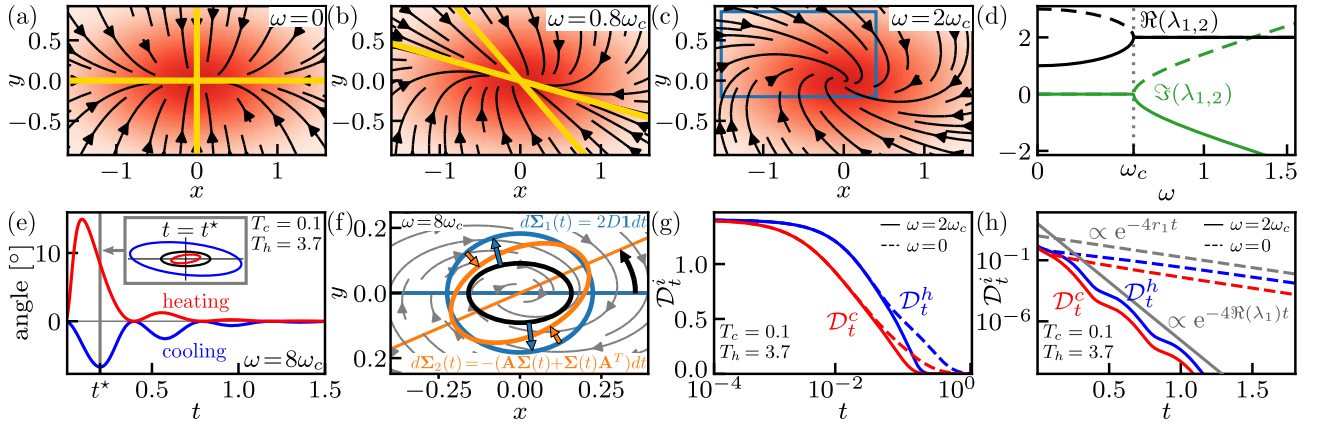
FIG. 2. (a-c) Steady-state density $p_s^w(\mathbf{x})$ (color gradient) and streamlines of the drift field $-\mathbf{A}\mathbf{x}$ for a 2d motion in Eq. (2) with $\boldsymbol{\sigma}_w = \sqrt{2}\mathbb{1}$ and drift matrix $\mathbf{A}$ with elements $A_{jj} = r_j$ with $r_1 = 1$, $r_2 = 3$, $A_{jk} = (-1)^j \omega r_k$ for $j, k \in \{1, 2\}$, with ω in units of $\omega_c \equiv |r_2 - r_1|/2\sqrt{r_1 r_2}$. Real eigendirections (yellow) only exist for $\omega \leq \omega_c$. (d) Real and imaginary parts of eigenvalues of $\mathbf{A}$ as a function of ω. At $\omega = \omega_c$ the eigenvalues coincide and eigendirections (yellow lines in b,c) merge, i.e. $\mathbf{A}$ is not diagonalizable. For $\omega > \omega_c$ the eigenvalues are complex. (e) Angle between the covariance matrices $\boldsymbol{\Sigma}_i^w(t)$ and $\boldsymbol{\Sigma}_{s,w}$. (f) Explanation of the counter-intuitive opposing (effective) rotations at small times during heating from $T_c/T_w = 0.1$. The change $d\boldsymbol{\Sigma}(t)$ in Eq. (4) starting from the initial $\boldsymbol{\Sigma}_{s,i}$ (black ellipse) for $dt = 0.05$ split into diffusive (yielding the blue ellipse) and drift along the grey streamlines (yielding orange ellipse) contributions. (g-h) $\mathcal{D}_t^i$ for heating and cooling with and without driving on logarithmic-linear and linear-logarithmic scales. The driven system relaxes faster at large t as predicted from the eigenvalues in (e). Grey lines in (h) show the limiting relaxation rates for long times, $e^{-4r_1 t}$ (dashed line) and $e^{-4\Re(\lambda_1)t}$ (solid line).

$\boldsymbol{\Sigma}_{s,i}$ as it is not of the form $\boldsymbol{\alpha}_i \boldsymbol{\Sigma}_{s,i}^{-1}$ with $\boldsymbol{\alpha}_i^T = -\boldsymbol{\alpha}_i$ (see [68] for details about the *consistent* comparison of equilibrium versus nonequilibrium).

We now consider influence of the non-equilibrium driving. For linear drift the relaxation is governed by the eigenvalues of $\mathbf{A}$ [96, 97]. Since $\boldsymbol{\Sigma}_{s,i}$ is, by definition, symmetric with positive eigenvalues, we can find a matrix $\boldsymbol{\beta} = \boldsymbol{\beta}^T$ such that $\boldsymbol{\beta}^2 \equiv \boldsymbol{\Sigma}_{s,i}^{-1}$ [98]. Thus, the matrix $\boldsymbol{\beta}\mathbf{D}_i\boldsymbol{\Sigma}_{s,i}^{-1}\boldsymbol{\beta}^{-1} = \boldsymbol{\beta}\mathbf{D}_i\boldsymbol{\beta} = \boldsymbol{\beta}\boldsymbol{\sigma}_i(\boldsymbol{\beta}\boldsymbol{\sigma}_i)^T/2$ is symmetric which alongside $\det(\boldsymbol{\beta}\boldsymbol{\sigma}_i) \neq 0$ implies that $\mathbf{D}_i\boldsymbol{\Sigma}_{s,i}^{-1}$ is diagonalizable with positive eigenvalues [99]. Therefore, in the absence of driving $\mathbf{A} = \mathbf{D}_i\boldsymbol{\Sigma}_{s,i}^{-1}$ expectedly has strictly positive eigenvalues reflecting a monotonous relaxation to equilibrium.

Once we include driving $\boldsymbol{\alpha}_w \neq 0$ in the steady-state-preserving form Eq. (7), the spectrum may or may not become complex depending on the detailed form of $\boldsymbol{\alpha}_w$, see e.g. Fig. 2a-d. Complex eigenvectors imply that eigendirections where the drift points "straight" towards $\mathbf{0}$ cease to exist, see Fig. 2a-c. This happens already at arbitrarily small driving if level sets of $p_s(\mathbf{x})$ are (hyper)spherical. If some eigenvalues are on the threshold of becoming complex (branching point ω_c in Fig. 2d), $\mathbf{A}$ may become non-diagonalizable. In terms of the minimal 2d example in Fig. 2 we have that $\mathbf{A}$ is non-diagonalizable when $\omega = \pm\omega_c$ (see Fig. 2d).

An interesting consequence of driving is that the different dimensions no longer decouple as they do under detailed balance (see Fig. 2a). This means that the d-dimensional Langevin equation (2) cannot be decomposed into 1d equations and that rotational dynamics may emerge. In the particular case of temperature

quenches we find that driving causes a time-dependent rotation of the level sets of $P_i^w(\mathbf{x}, t)$, see Fig. 2e. In agreement with the opposite sings of $T_i - T_w$ in Eq. (4), these rotations occur in opposite directions during heating and cooling, which is a striking new feature of the relaxation asymmetry. The asymmetry implies that thermal relaxation must *not* be understood as passing through local equilibria at intermediate (effective) temperatures [1], since this would imply a symmetric relaxation independent of the sign of the temperature quench. Moreover, the rotation in opposite directions emphasizes that heating and cooling here evolve along very distinct pathways in the space of probability distributions (see also [56]).

While the initial rotation during cooling follows the direction of driving, most surprisingly the effective rotations during heating initially oppose the direction of the driving (see Fig. 2e). This effect can be traced to the interplay of ("Trotterized" [100]) diffusion and drift during individual small time increments, see Fig. 2f. During heating for an increment dt diffusion alone propagates the black to the more circular blue ellipse. The subsequent drift along the elliptical streamlines propagates this blue ellipse to the orange ellipse that is, however, effectively rotated in the direction opposite to the drift (for further details see [68]).

Accelerated relaxation.—Before proving the relaxation asymmetry we discuss the acceleration of relaxation via driving [63–65, 67]. We therefore focus on the real part of the eigenvalues which determines the relaxation time-scales. Upon a change of basis we find $\widetilde{\mathbf{A}} \equiv \boldsymbol{\beta}\mathbf{A}\boldsymbol{\beta}^{-1} = \boldsymbol{\beta}\mathbf{D}_i\boldsymbol{\beta} + \boldsymbol{\beta}\boldsymbol{\alpha}_i\boldsymbol{\beta}$ where $(\boldsymbol{\beta}\boldsymbol{\alpha}_i\boldsymbol{\beta})^T = -\boldsymbol{\beta}\boldsymbol{\alpha}_i\boldsymbol{\beta}$. Then, for any complex eigenvalue λ of $\widetilde{\mathbf{A}}$ with eigenvector $\mathbf{v} \neq 0$ we

may write $2\Re(\lambda)\mathbf{v}^\dagger\mathbf{v} = (\lambda+\lambda^\dagger)\mathbf{v}^\dagger\mathbf{v} = \mathbf{v}^\dagger(\widetilde{\mathbf{A}}+\widetilde{\mathbf{A}}^\dagger)\mathbf{v} = 2\mathbf{v}^\dagger\boldsymbol{\beta}\mathbf{D}_i\boldsymbol{\beta}\mathbf{v}$, where $\dagger$ denotes the Hermitian adjoint. Decomposing $\mathbf{v}$, $\mathbf{v}^\dagger$ in the orthonormal eigenbasis of $\boldsymbol{\beta}\mathbf{D}_i\boldsymbol{\beta}$ with eigenvalues $0 < \mu_1 \leq \cdots \leq \mu_d$, we have with $c_j \in \mathbb{C}$

$$\Re(\lambda) = \frac{\mathbf{v}^\dagger\boldsymbol{\beta}\mathbf{D}_i\boldsymbol{\beta}\mathbf{v}}{\mathbf{v}^\dagger\mathbf{v}} = \frac{\sum_{j=1}^d c_j^\dagger c_j \mu_j}{\sum_{j=1}^d c_j^\dagger c_j} \in [\mu_1, \mu_d]. \quad (8)$$

This means that the real parts of the eigenvalues in the presence of driving remain not only positive, as required for the existence of a steady state, but even remain in the interval $[\mu_1, \mu_d]$. Thus, Eq. (8) states that the smallest real part of eigenvalues of $\mathbf{A}$ under driving obeys $\Re(\lambda_1) \geq \mu_1$. Note that $\Re(\lambda_1)$ typically [101] sets the slowest relaxation rate [96, 97]. Since $\Re(\lambda_1)$ increases (or does not decrease) upon driving, the latter typically enhances relaxation on long time scales, as already shown in [67].

Driving also affects the adiabatic entropy production. This effect, however, scales trivially, as the adiabatic entropy production increases with increasing $\boldsymbol{\alpha}_i$ according to $\boldsymbol{\alpha}_i^T\mathbf{D}_i^{-1}\boldsymbol{\alpha}_i$ [68]. Hence, there is *no direct connection* between faster relaxation and steady-state dissipation, as the influence of driving on the eigenvalues is specific. For example, the acceleration in $d=2$ saturates [see $\Re(\lambda_1)$ in Fig. 2d]. More drastically, multiplying $\boldsymbol{\alpha}_i$ by a factor larger than 1 in $d=3$ may decrease $\Re(\lambda_1)$ [67].

We see from Eq. (6) that $\mathbf{X}(t) \sim \mathrm{e}^{-2\Re(\lambda_1)t}$ for long times and therefore $\mathcal{D}_t^i \sim \mathrm{e}^{-4\Re(\lambda_1)t}$ (see [68] and Fig. 2g-h). The statement "accelerated relaxation", $\Re(\lambda_1) \geq \mu_1$, means that both, heating and cooling will at long times be faster. In general the *difference* between heating and cooling upon driving can become larger or smaller than for reversible dynamics with the same $\boldsymbol{\Sigma}_{s,i}$, but as we now prove heating is always faster than cooling.

Proof of relaxation asymmetry in driven systems.— We now prove the relaxation asymmetry for the dynamics in Eq. (2), i.e. $\Delta\mathcal{D}_t \equiv \mathcal{D}_t^h - \mathcal{D}_t^c > 0$ for all $t > 0$. By Eq. (6)

$$\Delta\mathcal{D}_t = \frac{\delta\tilde{T}_h - \delta\tilde{T}_c}{2}\,\mathrm{tr}\mathbf{X}(t) - \frac{1}{2}\ln\frac{\det\left[\mathbb{1}+\delta\tilde{T}_h\,\mathbf{X}(t)\right]}{\det\left[\mathbb{1}+\delta\tilde{T}_c\,\mathbf{X}(t)\right]}. \quad (9)$$

To prove the asymmetry we must understand the properties of $\mathbf{X}(t)$, which is T_i-independent. Using the steady-state Lyapunov equation (3) we can rewrite $\mathbf{X}(t)$ as

$$\mathbf{X}(t) = \mathrm{e}^{-\mathbf{A}t}\mathrm{e}^{-\mathbf{A}_{-\alpha}t}, \quad (10)$$

where $\mathbf{A}_{-\boldsymbol{\alpha}} \equiv (\mathbf{D}_w - \boldsymbol{\alpha}_w)\boldsymbol{\Sigma}_{s,w}^{-1}$ is the driving-reversed version of $\mathbf{A}$ as in Eq. (7). This form is reminiscent of the dual-reversal symmetry [77, 102–104] stating that time-reversal in non-equilibrium steady states requires concurrent current reversal. Eq. (10) is illustrated in Fig. 3a. The proof again requires to change the basis via $\boldsymbol{\beta}$ as

$$\widetilde{\mathbf{X}}(t) \equiv \boldsymbol{\beta}\mathbf{X}(t)\boldsymbol{\beta}^{-1} = \mathrm{e}^{-\widetilde{\mathbf{A}}t}\left(\mathrm{e}^{-\widetilde{\mathbf{A}}t}\right)^T, \quad (11)$$

where we used $\boldsymbol{\beta}\mathbf{A}_{-\alpha}\boldsymbol{\beta}^{-1} = \widetilde{\mathbf{A}}^T$ and $\mathrm{e}^{-\widetilde{\mathbf{A}}^T t} = (\mathrm{e}^{-\widetilde{\mathbf{A}}t})^T$. Thus, $\widetilde{\mathbf{X}}(t)$ is symmetric and hence diagonalizable with
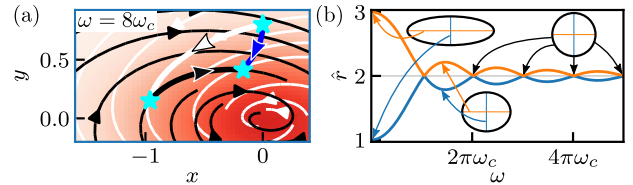
FIG. 3. (a) Illustration of Eq. (10): Streamplot of the drift field $-\mathbf{A}\mathbf{x}$ (black) as in blue frame in Fig. 2c, and inverted drift field $-\mathbf{A}_{-\alpha}\mathbf{x}$ (white). The white line depicts $\mathrm{e}^{-\mathbf{A}_{-\alpha}\tau}\mathbf{x}_0$ for $\tau \in [0,t]$, the black line is $\mathrm{e}^{-\mathbf{A}\tau}\mathrm{e}^{-\mathbf{A}_{-\alpha}t}\mathbf{x}_0$, and the blue line shows $\mathbf{X}(\tau)\mathbf{x}_0$. (b) Effective stiffness $\hat{r}_j(\omega) \equiv -\ln(x_j^t)/2t$ at $t=1$ as a function of driving ω (see [68]). For large driving the directions mix, such that the system effectively approaches a circular parabola with stiffness $(r_1+r_2)/2$, which is the real part of eigenvalues in Fig. 2d.

real eigenvalues. Since, $\det\mathrm{e}^{-\widetilde{\mathbf{A}}t} = \mathrm{e}^{-\mathrm{tr}\widetilde{\mathbf{A}}t}$, we have $\det\widetilde{\mathbf{X}}(t) = \mathrm{e}^{-2\mathrm{tr}\widetilde{\mathbf{A}}t} \neq 0$. Therefore, $\widetilde{\mathbf{X}}(t)$ and thus $\mathbf{X}(t)$ have positive eigenvalues $x_j^t > 0$, $j = 1,\ldots,d$ [99]. Although $\mathbf{A}$ may have complex eigenvalues or even be non-diagonalizable and $\exp(-\mathbf{A}t)$ may be rotational (see Figs. 2c and 3a), $\mathbf{X}(t)$ has a real eigensystem since consecutive rotations in forward and current-reversed directions effectively cancel rotations, see Eq. (10) and Fig. 3a.

Using the eigenvalues $x_j^t > 0$ we rewrite Eq. (9) as

$$\Delta\mathcal{D}_t = \sum_{j=1}^d\left(\frac{\delta\tilde{T}_h - \delta\tilde{T}_c}{2}x_j^t - \frac{1}{2}\ln\left[\frac{1+\delta\tilde{T}_h x_j^t}{1+\delta\tilde{T}_c x_j^t}\right]\right). \quad (12)$$

If all $x_j^t \in (0,1)$, the proof for reversible systems [57, 61] asserts that $\Delta\mathcal{D}_t > 0$. It therefore suffices to show that $x_j^t < 1$ for all j, which is equivalent to $||\mathbf{X}(t)|| < 1$, where $||\mathbf{M}|| \equiv \sup_{\mathbf{v}\in\mathbb{R}^d\setminus\mathbf{0}}||\mathbf{M}\mathbf{v}||_2/||\mathbf{v}||_2$ and $||\mathbf{v}||_2 = \sqrt{\mathbf{v}^T\mathbf{v}}$ are the matrix and Euclidean norm, respectively. Eq. (10) does not help in showing this [105]; although eigenvalues of $\mathbf{A}$ have positive real parts [see Eq. (8)], it may be that $||\mathrm{e}^{-\mathbf{A}\pm\alpha t}|| > 1$ (e.g. the distance to $\mathbf{0}$ in Fig. 3a increases along the white line). This is possible because the eigenvectors of $\mathbf{A}$ are not orthogonal.

We thus change the basis as in Eq. (11) and use the log-norm inequality $||\exp(\mathbf{M}t)|| \leq \exp[\mu(\mathbf{M})t]$ [106] with log norm $\mu(\mathbf{M}) \equiv \lim_{h\to 0^+} h^{-1}(||\mathbb{1}+h\mathbf{M}|| - 1)$ yielding $\mu(-\widetilde{\mathbf{A}}) \equiv \mu(-\boldsymbol{\beta}\mathbf{A}\boldsymbol{\beta}^{-1}) = \mu(-\boldsymbol{\beta}\mathbf{D}_w\boldsymbol{\beta}) = -\mu_1$ determined by the symmetric part $(\widetilde{\mathbf{A}}+\widetilde{\mathbf{A}}^T)/2 = \boldsymbol{\beta}\mathbf{D}_w\boldsymbol{\beta}$ [68]. This basis is appropriate because $\boldsymbol{\beta}\boldsymbol{\alpha}_w\boldsymbol{\beta}$ in $\widetilde{\mathbf{A}}$ (unlike $\boldsymbol{\alpha}_w\boldsymbol{\Sigma}_{s,w}^{-1}$ in $\mathbf{A}$) has no symmetric part, i.e. the driving only affects the rotational part. The log-norm inequality thus implies $||\exp(-\widetilde{\mathbf{A}}t)|| \leq \exp[\mu(-\widetilde{\mathbf{A}})t] = \exp(-\mu_1 t)$ and similarly $||\exp(-\widetilde{\mathbf{A}}^T t)|| \leq \exp(-\mu_1 t)$, and by the submultiplicative property of the matrix norm we obtain from Eq. (11)

$$||\widetilde{\mathbf{X}}(t)|| \leq \left\|\mathrm{e}^{-\widetilde{\mathbf{A}}t}\right\|\left\|\left(\mathrm{e}^{-\widetilde{\mathbf{A}}t}\right)^T\right\| \leq \mathrm{e}^{-2\mu_1 t} < 1. \quad (13)$$

Since $||\widetilde{\mathbf{X}}(t)|| = ||\mathbf{X}(t)||$ this implies $x_j^t < 1$ and with Eq. (12) completes the proof of $\Delta\mathcal{D}_t > 0$ for all $t > 0$.

The proof provides important insight into the thermodynamics of the asymmetry in reversible versus driven systems. Namely, $\Delta\mathcal{D}_t$ in Eq. (12) for a driven system at any t is equal to that of any reversible system with drift matrix $\hat{\mathbf{A}}$ having eigenvalues $\hat{\mu}_i$ satisfying $\mathrm{e}^{-2\hat{\mu}_j t} = x_j^t$. Therefore, at each t the relaxation asymmetry of a driven system is isomorphic to that of an equilibrium system with different geometry (see Fig. 3b for effective stiffness axes of the 2-dimensional parabolic potential), which implies the persistence of the asymmetry. This provokes intriguing questions about the existence of the asymmetry in the presence of time-dependent driving.

Conclusion.—We have proven that overdamped ergodic systems driven by linear drift, conservative or not, for any pair of thermodynamically equidistant temperature quenches warm up faster than they cool down. The relaxation asymmetry [57], which was recently confirmed experimentally [56], therefore persists in driven systems. As the original proof hinged on microscopic reversibility, this finding is surprising and is explained by a non-trivial isomorphism between driven and reversible processes. In the presence of driving a striking new feature of the relaxation asymmetry appears: rotational dynamics emerge with opposite directions during heating and cooling, respectively. This further highlights that small, noisy systems do *not* relax by passing through local equilibria [1]. Moreover, rotations in opposing directions emphasize that heating and cooling evolve along fundamentally distinct pathways [56]. An analysis with the framework of "thermal kinematics" [56] will bring even deeper insight. Our results motivate further studies on the existence of the relaxation asymmetry in temporally driven systems [49, 107–111], systems with nonlinear drift [25, 27, 28, 30, 112], and in the presence of inertial effects [35].

[1] S. R. de Groot and P. Mazur, *Non-equilibrium Thermodynamics*, 2nd ed. (North-Holland, Amsterdam, 1962).
[2] L. Onsager, Phys. Rev. **37**, 405 (1931).
[3] L. Onsager, Phys. Rev. **38**, 2265 (1931).
[4] R. Kubo, M. Yokota, and S. Nakajima, J. Phys. Soc. Jpn. **12**, 1203 (1957).
[5] M. Baiesi and C. Maes, New J. Phys. **15**, 013004 (2013).
[6] C. Maes, K. Netočný, and B. Wynants, Phys. Rev. Lett. **107**, 010601 (2011).
[7] M. Polettini and M. Esposito, Phys. Rev. E **88**, 012112 (2013).
[8] L. Bertini, A. De Sole, D. Gabrielli, G. Jona-Lasinio, and C. Landim, J. Stat. Phys. **116**, 831 (2004).
[9] L. Bertini, A. De Sole, D. Gabrielli, G. Jona-Lasinio, and C. Landim, Rev. Mod. Phys. **87**, 593 (2015).
[10] R. S. Maier and D. L. Stein, Phys. Rev. E **48**, 931 (1993).
[11] F. Bouchet and J. Reygner, Ann. Henri Poincare **17**, 3499 (2016).
[12] J. Casademunt, R. Mannella, P. V. E. McClintock, F. E. Moss, and J. M. Sancho, Phys. Rev. A **35**, 5183 (1987).
[13] I. M. Sokolov, Phys. Rev. E **66**, 041101 (2002).
[14] I. M. Sokolov, Phys. Rev. Lett. **90**, 080601 (2003).
[15] B. Dybiec, I. M. Sokolov, and A. V. Chechkin, Commun. Nonlinear Sci. Numer. Simul. **16**, 4549–4557 (2011).
[16] D. E. Makarov, J. Chem. Phys. **138**, 014102 (2013).
[17] R. Satija and D. E. Makarov, J. Phys. Chem. B **123**, 802–810 (2019).
[18] A. Lapolla and A. Godec, Front. Phys. **7**, 182 (2019).
[19] A. Lapolla and A. Godec, J. Chem. Phys. **153**, 194104 (2020).
[20] P. Talkner and P. Hänggi, Rev. Mod. Phys. **92**, 041002 (2020).
[21] C. Ayaz, L. Scalfi, B. A. Dalton, and R. R. Netz, Phys. Rev. E **105**, 054138 (2022).
[22] L. F. Cugliandolo, D. S. Dean, and J. Kurchan, Phys. Rev. Lett. **79**, 2168 (1997).
[23] E. Lippiello, M. Baiesi, and A. Sarracino, Phys. Rev. Lett. **112**, 140602 (2014).
[24] A. Gal and O. Raz, Phys. Rev. Lett. **124**, 060602 (2020).
[25] Z. Lu and O. Raz, Proc. Natl. Acad. Sci. U.S.A. **114**, 5083 (2017).
[26] A. Lasanta, F. Vega Reyes, A. Prados, and A. Santos, Phys. Rev. Lett. **119**, 148001 (2017).
[27] M. Baity-Jesi, E. Calore, A. Cruz, L. A. Fernandez, J. M. Gil-Narvión, A. Gordillo-Guerrero, D. Iñiguez, A. Lasanta, A. Maiorano, E. Marinari, V. Martin-Mayor, J. Moreno-Gordo, A. M. Sudupe, D. Navarro, G. Parisi, S. Perez-Gaviro, F. Ricci-Tersenghi, J. J. Ruiz-Lorenzo, S. F. Schifano, B. Seoane, A. Tarancón, R. Tripiccione, and D. Yllanes, Proc. Natl. Acad. Sci. U.S.A. **116**, 15350 (2019).
[28] A. Kumar and J. Bechhoefer, Nature **584**, 64 (2020).
[29] F. Carollo, A. Lasanta, and I. Lesanovsky, Phys. Rev. Lett. **127**, 060401 (2021).
[30] A. Kumar, R. Chétrite, and J. Bechhoefer, Proc. Natl. Acad. Sci. U.S.A. **119**, e2118484119 (2022).
[31] I. Klich, O. Raz, O. Hirschberg, and M. Vucelja, Phys. Rev. X **8**, 021060 (2019).
[32] R. Holtzman and O. Raz, Commun. Phys. **5**, 280 (2022).
[33] J. Degünther and U. Seifert, Europhys. Lett. **139**, 41002 (2022).
[34] I. L. Morgan, R. Avinery, G. Rahamim, R. Beck, and O. A. Saleh, Phys. Rev. Lett. **125**, 058001 (2020).
[35] A. Militaru, A. Lasanta, M. Frimmer, L. L. Bonilla, L. Novotny, and R. A. Rica, Phys. Rev. Lett. **127**, 130603 (2021).
[36] F. Bouchet, K. Gawedzki, and C. Nardini, J. Stat. Phys. **163**, 1157–1210 (2016).
[37] Y. Baek and Y. Kafri, J. Stat. Mech. **2015**, P08026 (2015).
[38] J. P. Garrahan, R. L. Jack, V. Lecomte, E. Pitard, K. van Duijvendijk, and F. van Wijland, Phys. Rev. Lett. **98**, 195702 (2007).
[39] T. Speck, A. Engel, and U. Seifert, J. Stat. Mech. **2012**, P12001 (2012).
[40] P. Tsobgni Nyawo and H. Touchette, Europhys. Lett.

116, 50009 (2016).

[41] V. Ermolaev and C. Külske, J. Stat. Phys. **141**, 727–756 (2010).

[42] J. Meibohm and M. Esposito, Phys. Rev. Lett. **128**, 110603 (2022).

[43] J. Meibohm and M. Esposito, New J. Phys. **25**, 023034 (2023).

[44] K. Blom and A. Godec, Global speed limit for finite-time dynamical phase transition in nonequilibrium relaxation (2022).

[45] P. Pietzonka, F. Ritort, and U. Seifert, Phys. Rev. E **96**, 012101 (2017).

[46] A. Dechant and S.-i. Sasa, J. Stat. Mech. **2018**, 063209 (2018).

[47] K. Liu, Z. Gong, and M. Ueda, Phys. Rev. Lett. **125**, 140602 (2020).

[48] T. Koyuk and U. Seifert, Phys. Rev. Lett. **122**, 230601 (2019).

[49] T. Koyuk and U. Seifert, Phys. Rev. Lett. **125**, 260604 (2020).

[50] C. Dieball and A. Godec, Phys. Rev. Lett. **130**, 087101 (2023).

[51] N. Shiraishi, K. Funo, and K. Saito, Phys. Rev. Lett. **121**, 070601 (2018).

[52] E. Aurell, C. Mejía-Monasterio, and P. Muratore-Ginanneschi, Phys. Rev. Lett. **106**, 250601 (2011).

[53] K. Yoshimura and S. Ito, Phys. Rev. Lett. **127**, 160601 (2021).

[54] S. Ito and A. Dechant, Phys. Rev. X **10**, 021056 (2020).

[55] N. Shiraishi and K. Saito, Phys. Rev. Lett. **123**, 110603 (2019).

[56] M. Ibáñez, C. Dieball, A. Lasanta, A. Godec, and R. A. Rica, Heating and cooling are fundamentally asymmetric and evolve along distinct pathways (2023).

[57] A. Lapolla and A. Godec, Phys. Rev. Lett. **125**, 110602 (2020).

[58] T. V. Vu and Y. Hasegawa, Phys. Rev. Res. **3**, 043160 (2021).

[59] S. K. Manikandan, Phys. Rev. Res. **3**, 043108 (2021).

[60] J. Meibohm, D. Forastiere, T. Adeleke-Larodo, and K. Proesmans, Phys. Rev. E **104**, L032105 (2021).

[61] A. Lapolla and A. Godec, Phys. Rev. Lett. **128**, 229901 (2022).

[62] C.-R. Hwang, S.-Y. Hwang-Ma, and S.-J. Sheu, Ann. Appl. Probab. **15**, 1433 (2005).

[63] S. C. Kapfer and W. Krauth, Phys. Rev. Lett. **119**, 240603 (2017).

[64] L. Rey-Bellet and K. Spiliopoulos, Nonlinearity **28**, 2081 (2015).

[65] F. Coghi, R. Chetrite, and H. Touchette, Phys. Rev. E **103**, 062142 (2021).

[66] H. Qian, J. Math. Phys. **54**, 053302 (2013).

[67] C.-R. Hwang, S.-Y. Hwang-Ma, and S.-J. Sheu, Ann. Appl. Probab. **3**, 897 (1993).

[68] See Supplemental Material at [. . .].

[69] J. L. Lebowitz and P. G. Bergmann, Ann. Phys. **1**, 1 (1957).

[70] M. C. Mackey, Rev. Mod. Phys. **61**, 981 (1989).

[71] S. Vaikuntanathan and C. Jarzynski, Europhys. Lett. **87**, 60005 (2009).

[72] M. Esposito and C. Van den Broeck, Phys. Rev. Lett. **104**, 090601 (2010).

[73] C. Van den Broeck and M. Esposito, Phys. Rev. E **82**, 011144 (2010).

[74] S. Kullback and R. A. Leibler, Ann. Math. Stat. **22**, 79 (1951).

[75] N. Ikeda and S. Watanabe, *Stochastic Differential Equations and Diffusion Processes*, 1st ed. (North Holland, 1981) eBook ISBN: 9780080960128.

[76] C. W. Gardiner, *Handbook of Stochastic Methods for Physics, Chemistry, and the Natural Sciences* (Springer-Verlag, Berlin New York, 1985).

[77] C. Dieball and A. Godec, Phys. Rev. Research **4**, 033243 (2022).

[78] As $\boldsymbol{\Sigma}_{\mathrm{s},i}$ is invertible and symmetric Eq. (3) $\boldsymbol{\alpha}_i = (\mathbf{A} - \mathbf{D}_i \boldsymbol{\Sigma}_{\mathrm{s},i}^{-1}) \boldsymbol{\Sigma}_{\mathrm{s},i} = -\boldsymbol{\Sigma}_{\mathrm{s},i} (\mathbf{A}^T - \boldsymbol{\Sigma}_{\mathrm{s},i}^{-1} \mathbf{D}_i) = -\boldsymbol{\alpha}_i^T$. In fact $\boldsymbol{\Sigma}_{\mathrm{s},i}^{-1} \mathbf{x}$ and $\boldsymbol{\alpha}_i \boldsymbol{\Sigma}_{\mathrm{s},i}^{-1} \mathbf{x}$ are orthogonal since their scalar product yields an antisymmetric quadratic form $\mathbf{x}^T \boldsymbol{\Sigma}_{\mathrm{s},i}^{-1} \boldsymbol{\alpha}_i \boldsymbol{\Sigma}_{\mathrm{s},i}^{-1} \mathbf{x} = 0$ [66].

[79] U. Seifert, Rep. Prog. Phys. **75**, 126001 (2012).

[80] B. H. Zimm, J. Chem. Phys. **24**, 269 (1956).

[81] M. Doi and S. F. Edwards, *The Theory of Polymer Dynamics*, International Series of Monographs on Physics (Clarendon Press, Oxford, England, 1988).

[82] R. R. Cheng, A. T. Hawk, and D. E. Makarov, J. Chem. Phys. **138**, 074112 (2013).

[83] A. Soranno, B. Buchli, D. Nettels, R. R. Cheng, S. Müller-Späth, S. H. Pfeil, A. Hoffmann, E. A. Lipman, D. E. Makarov, and B. Schuler, Proc. Natl. Acad. Sci. U.S.A. **109**, 17800 (2012).

[84] B. Schuler, A. Soranno, H. Hofmann, and D. Nettels, Annu. Rev. Biophys. **45**, 207 (2016).

[85] J. O. Daldrop, J. Kappler, F. N. Brünig, and R. R. Netz, Proc. Natl. Acad. Sci. U.S.A. **115**, 5169 (2018).

[86] D. E. Smith, H. P. Babcock, and S. Chu, Science **283**, 1724 (1999).

[87] S. Gerashchenko and V. Steinberg, Phys. Rev. Lett. **96**, 038304 (2006).

[88] P. S. Doyle, B. Ladoux, and J.-L. Viovy, Phys. Rev. Lett. **84**, 4769 (2000).

[89] T. T. Perkins, D. E. Smith, R. G. Larson, and S. Chu, Science **268**, 83 (1995).

[90] C. Schroeder, R. Teixeira, E. Shaqfeh, and S. Chu, Phys. Rev. Lett. **95**, 018301 (2005).

[91] R. E. Teixeira, H. P. Babcock, E. S. G. Shaqfeh, and S. Chu, Macromolecules **38**, 581 (2005).

[92] M. Harasim, B. Wunderlich, O. Peleg, M. Kröger, and A. R. Bausch, Phys. Rev. Lett. **110**, 108302 (2013).

[93] A. Alexander-Katz, M. F. Schneider, S. W. Schneider, A. Wixforth, and R. R. Netz, Phys. Rev. Lett. **97**, 138101 (2006).

[94] T. T. Perkins, D. E. Smith, and S. Chu, Science **276**, 2016 (1997).

[95] Y. Roichman, B. Sun, A. Stolarski, and D. G. Grier, Phys. Rev. Lett. **101**, 128301 (2008).

[96] G. Metafune, Ann. Scuola Norm. Sup. Pisa Cl. Sci. (4) **30**, 97 (2001).

[97] G. Metafune, D. Pallara, and E. Priola, J. Funct. Anal. **196**, 40 (2002).

[98] From the orthogonal diagonalization $\mathbf{O} \boldsymbol{\Sigma}_{\mathrm{s},i}^{-1} \mathbf{O}^T = \mathrm{diag}(s_j)$ we define $\boldsymbol{\beta} \equiv \mathbf{O}^T \mathrm{diag}_{\sqrt{s_j}} \mathbf{O}$.

[99] Any matrix of the form $\mathbf{M}\mathbf{M}^T$ is symmetric, and therefore diagonalizable, with real non-negative eigenvalues, since $\mathbf{M}\mathbf{M}^T \mathbf{v} = \lambda \mathbf{v}$ implies $\lambda = \mathbf{v}^T \mathbf{M}\mathbf{M}^T \mathbf{v}/\mathbf{v}^T \mathbf{v} = (\mathbf{M}^T \mathbf{v})^T \mathbf{M}^T \mathbf{v}/\mathbf{v}^T \mathbf{v} \geq 0$.

[100] H. F. Trotter, Proc. Amer. Math. Soc. **10**, 545 (1959).

[101] Unless the initial distribution has only a negligible pro-

jection onto the slowest modes.

[102] T. Hatano and S.-i. Sasa, Phys. Rev. Lett. **86**, 3463 (2001).

[103] A. Dechant and S.-i. Sasa, Phys. Rev. Research **3**, 042012 (2021).

[104] C. Dieball and A. Godec, Phys. Rev. Lett. **129**, 140601 (2022).

[105] Eq. (10) suffices only at equilibrium $\mathbf{A} = \mathbf{A}_{-\boldsymbol{\alpha}} = \mathbf{D}_w \boldsymbol{\Sigma}_{\mathrm{s},w}^{-1}$ where $\mathbf{X}(t) = \exp(-2\mathbf{D}_w \boldsymbol{\Sigma}_{\mathrm{s},w}^{-1} t)$ decomposes into $x_j^t = \exp(-2\mu_j t) < 1$.

[106] G. Dahlquist, *Stability and Error Bounds in the Numerical Integration of Ordinary Differential Equations* (Almqvist & Wiksell, Uppsala, Sweden, 1958).

[107] V. Blickle and C. Bechinger, Nat. Phys. **8**, 143 (2012).

[108] I. A. Martínez, É. Roldán, L. Dinis, D. Petrov, and R. A. Rica, Phys. Rev. Lett. **114**, 120601 (2015).

[109] I. A. Martínez, É. Roldán, L. Dinis, D. Petrov, J. M. Parrondo, and R. A. Rica, Nat. Phys. **12**, 67 (2016).

[110] S. Krishnamurthy, S. Ghosh, D. Chatterji, R. Ganapathy, and A. Sood, Nat. Phys. **12**, 1134 (2016).

[111] M. Rademacher, M. Konopik, M. Debiossac, D. Grass, E. Lutz, and N. Kiesel, Phys. Rev. Lett. **128**, 070601 (2022).

[112] J. Gladrow, M. Ribezzi-Crivellari, F. Ritort, and U. F. Keyser, Nat. Commun. **10**, 55 (2019).

Supplemental Material for:
Asymmetric Thermal Relaxation in Driven Systems: Rotations go Opposite Ways

Cai Dieball[1], Gerrit Wellecke[1,2] and Aljaž Godec[1]

[1]*Mathematical bioPhysics Group, Max Planck Institute for Multidisciplinary Sciences, 37077 Göttingen, Germany*
[2]*Present address: Theory of Biological Fluids, Max Planck Institute for Dynamics and Self-Organization, Göttingen 37077, Germany*

In this Supplementary Material we provide further details on model examples, arguments, and calculations presented in the Letter. Besides several technical details, we give the equations and parameters describing the the Rouse chain in confined shear flow and derive and solve equations for the covariance. We extensively elaborate on the rotations in different directions, and address the consistent comparison of equilibrium and non-equilibrium steady states. We conclude with a discussion of the log-norm inequality.

CONTENTS

I. ROUSE POLYMER WITH HYDRODYNAMIC INTERACTIONS AND INTERNAL FRICTION IN CONFINED SHEAR FLOW

In Fig. 1 in the Letter we consider the motivating example of a polymer chain with $N = 20$ beads in $3d$ space represented by the Rouse model with internal friction and hydrodynamic interactions in shear flow. That is, we assume that the beads are connected by harmonic springs with zero rest length [Eq. (S1)] and additionally interact via hydrodynamic interactions [Eq. (S3)] and experience internal friction [Eq. (S4)]. The chain is confined in a parabolic potential and is subject to a shear flow [Eqs. (S8)-(S9)]. We now describe the interactions and evolution equations individually, with increasing complexity.

In the classical Rouse model (i.e. without hydrodynamic interactions, internal friction, confinement and shear), the time-dependent position of the beads $\mathbf{x}_t$ is described by the $3N$ dimensional Langevin equation (denoting the spring stiffness by κ and solvent friction by γ)

$$\gamma d\mathbf{x}_t = -\kappa \mathbf{k}\mathbf{x}_t dt + \sqrt{2D_i} d\mathbf{W}_t, \tag{S1}$$

where the connectivity matrix $\mathbf{k}$ is a $3N \times 3N$ matrix that reads ($\mathbb{1}_3$ is the 3d unit matrix and all terms not shown

are 0)

$$\mathbf{k} = \begin{bmatrix} \mathbb{1}_3 & -\mathbb{1}_3 & & & & \\ -\mathbb{1}_3 & 2\mathbb{1}_3 & -\mathbb{1}_3 & & & 0 \\ & -\mathbb{1}_3 & 2\mathbb{1}_3 & -\mathbb{1}_3 & & \\ & & \cdots & \cdots & & \\ & & & \cdots & \cdots & \\ 0 & & & -\mathbb{1}_3 & 2\mathbb{1}_3 & -\mathbb{1}_3 \\ & & & & -\mathbb{1}_3 & \mathbb{1}_3 \end{bmatrix}. \tag{S2}$$

Note that the temperature dependence is contained in the diffusion constant $D_i \propto T_i$ as described in the Letter. Following Ref. [1], we introduce hydrodynamic interactions in the pre-averaging approximation via the $3N \times 3N$ matrix $\mathbf{H}$ with 3×3 entries for $m, n = 1, \ldots, N$

$$H_{mn} = \gamma^{-1} \mathbb{1}_3 \times \begin{cases} 1 & \text{if } n = m \\ \frac{1}{2\pi^2 \gamma |n-m|^{1/2}} & \text{if } n \neq m \end{cases}, \tag{S3}$$

and also include internal friction with friction parameter ξ_{IF}, such that the equation of motion of the chain becomes

$$d\mathbf{x}_t = \mathbf{H} \left(-\kappa \mathbf{k} \mathbf{x}_t dt - \xi_{\mathrm{IF}} \mathbf{k} d\mathbf{x}_t + \sqrt{2D_i} d\mathbf{W}_t \right). \tag{S4}$$

We now introduce a spatial confinement via a $3d$ harmonic potential centered at $\mathbf{x} = \mathbf{0}$ and subject the confined chain to a shear flow in the x-y-plane. To account for the confinement, we consider the three-dimensional matrix ($r_i > 0$)

$$\mathbf{C} = \mathbf{R}(\theta) \begin{bmatrix} r_x & 0 & 0 \\ 0 & r_y & 0 \\ 0 & 0 & r_z \end{bmatrix} \mathbf{R}(\theta)^T, \tag{S5}$$

and for the shear flow in the x-y-plane

$$\mathbf{S} = \begin{bmatrix} 0 & \omega & 0 \\ 0 & 0 & 0 \\ 0 & 0 & 0 \end{bmatrix}. \tag{S6}$$

Note that by introducing the shear flow $\mathbf{S}$ to the system, the microscopic reversibility is lost, i.e., we have an example that is genuinely driven out of equilibrium.

To avoid the special case where shear and confinement are orthogonal, we introduce the rotation matrix $\mathbf{R}(\theta)$ to rotate the confinement by an angle θ within the x-y-plane,

$$\mathbf{R}(\theta) = \begin{bmatrix} \cos(\theta) & -\sin(\theta) & 0 \\ \sin(\theta) & \cos(\theta) & 0 \\ 0 & 0 & 1 \end{bmatrix}. \tag{S7}$$

Now consider a $3N$ dimensional matrix $\mathbf{M}$ with $\mathbf{R}(\theta)\mathbf{C}\mathbf{R}^T(\theta) + \mathbf{S}$ on the N diagonal 3×3 blocks to impose the confinement and shear on each bead. Then the equation of motion for the confined polymer in shear flow reads

$$d\mathbf{x}_t = \mathbf{H} \left(-(\kappa \mathbf{k} + \mathbf{M})\mathbf{x}_t dt - \xi_{\mathrm{IF}} \mathbf{k} d\mathbf{x}_t + \sqrt{2D_i} d\mathbf{W}_t \right). \tag{S8}$$

This may now be rewritten as

$$\left(\mathbf{H}^{-1} + \xi_{\mathrm{IF}} \mathbf{k} \right) d\mathbf{x}_t = -(\kappa \mathbf{k} + \mathbf{M})\mathbf{x}_t dt + \sqrt{2D_i} d\mathbf{W}_t,$$
$$d\mathbf{x}_t = -\left(\mathbf{H}^{-1} + \xi_{\mathrm{IF}} \mathbf{k} \right)^{-1} (\kappa \mathbf{k} + \mathbf{M})\mathbf{x}_t dt + \sqrt{2D_i} \left(\mathbf{H}^{-1} + \xi_{\mathrm{IF}} \mathbf{k} \right)^{-1} d\mathbf{W}_t. \tag{S9}$$

Upon identifying

$$\mathbf{A} = \left(\mathbf{H}^{-1} + \xi_{\mathrm{IF}} \mathbf{k} \right)^{-1} (\kappa \mathbf{k} + \mathbf{M}), \quad \boldsymbol{\sigma}_i = \sqrt{2D_i} \left(\mathbf{H}^{-1} + \xi_{\mathrm{IF}} \mathbf{k} \right)^{-1} \tag{S10}$$

we arrive at the desired form $d\mathbf{x}_t = -\mathbf{A}\mathbf{x}_t dt + \boldsymbol{\sigma}_i d\mathbf{W}_t$ as described in the Letter.

The parameters used in Fig. 1 are $N = 20$, $r_x = 0$, $r_y = 0.1$, $r_z = 1$, $\theta = -10°$, $\gamma = 1$, $\xi_{\mathrm{IF}} = 1$, $D_w = 1$, $\kappa = 1$, $T_c = 0.05T_w$, $T_h = 4.56T_w$. In Fig. 1a we choose $\omega = 3$ while in Fig. 1b we use $\omega = 20$ to emphasize the differences between the curves. For the chosen parameters, several eigenvalues of the matrix $\mathbf{A}$ become complex, thus confirming that the Rouse model in the shear flow is an irreversible process.

II. LYAPUNOV EQUATION AND TIME-DEPENDENT COVARIANCE

Here we derive Eqs. (3) and (4) in the Letter. We consider dynamics governed by $d\mathbf{x}_t = -\mathbf{A}\mathbf{x}_t dt + \boldsymbol{\sigma} d\mathbf{W}_t$ as in Eq. (2) in the Letter. Taking the mean value gives $\frac{d}{dt}\langle \mathbf{x}_t \rangle = -\mathbf{A}\langle \mathbf{x}_t \rangle$ which implies $\langle \mathbf{x}_t \rangle = \mathrm{e}^{-\mathbf{A}t}\langle \mathbf{x}_0 \rangle$. In the Letter we only consider initial conditions with $\langle \mathbf{x}_0 \rangle = \mathbf{0}$ such that for all times $\langle \mathbf{x}_t \rangle = 0$. The covariance $\boldsymbol{\Sigma}(t) \equiv \langle \mathbf{x}_t \mathbf{x}_t^T \rangle - \langle \mathbf{x}_t \rangle \langle \mathbf{x}_t^T \rangle = \langle \mathbf{x}_t \mathbf{x}_t^T \rangle$ is always symmetric $\boldsymbol{\Sigma}(t)^T = \boldsymbol{\Sigma}(t)$ with strictly positive eigenvalues. Using Itô's Lemma [2, 3] we see that $\boldsymbol{\Sigma}(t)$ obeys the differential Lyapunov equation

$$
\begin{aligned}
\frac{d}{dt}\boldsymbol{\Sigma}(t) &= \langle d\mathbf{x}_t \mathbf{x}_t^T \rangle + \langle \mathbf{x}_t d\mathbf{x}_t^T \rangle + \langle d\mathbf{x}_t d\mathbf{x}_t^T \rangle \\
&= -\mathbf{A}\langle \mathbf{x}_t \mathbf{x}_t^T \rangle - \langle \mathbf{x}_t \mathbf{x}_t^T \rangle \mathbf{A}^T + \boldsymbol{\sigma}\boldsymbol{\sigma}^T \\
&= -\mathbf{A}\boldsymbol{\Sigma}(t) - \boldsymbol{\Sigma}(t)\mathbf{A}^T + 2\mathbf{D}.
\end{aligned}
\tag{S11}
$$

In the steady state (i.e. for $\mathbf{A}$ originating from a confining potential and $t \to \infty$) this approaches the steady-state covariance $\boldsymbol{\Sigma}_\mathrm{s}$ obeying the algebraic (i.e. non-differential) Lyapunov equation (Eq. (3) in the Letter, see also Ref. [3])

$$
\mathbf{A}\boldsymbol{\Sigma}_\mathrm{s} + \boldsymbol{\Sigma}_\mathrm{s}\mathbf{A}^T = 2\mathbf{D}.
\tag{S12}
$$

Given the solution $\boldsymbol{\Sigma}_\mathrm{s}$ of Eq. (S12), the solution for Eq. (S11) for an initial condition with covariance $\boldsymbol{\Sigma}(0)$ is obtained as

$$
\boldsymbol{\Sigma}(t) = \boldsymbol{\Sigma}_\mathrm{s} + \mathrm{e}^{-\mathbf{A}t}\left[\boldsymbol{\Sigma}(0) - \boldsymbol{\Sigma}_\mathrm{s}\right]\mathrm{e}^{-\mathbf{A}^T t}.
\tag{S13}
$$

This is proven by taking the derivative of the ansatz,

$$
\begin{aligned}
\frac{d}{dt}&\left(\boldsymbol{\Sigma}_\mathrm{s} + \mathrm{e}^{-\mathbf{A}t}\left[\boldsymbol{\Sigma}(0) - \boldsymbol{\Sigma}_\mathrm{s}\right]\mathrm{e}^{-\mathbf{A}^T t}\right) \\
&= -\mathbf{A}\left(\mathrm{e}^{-\mathbf{A}t}\left[\boldsymbol{\Sigma}(0) - \boldsymbol{\Sigma}_\mathrm{s}\right]\mathrm{e}^{-\mathbf{A}^T t}\right) - \left(\mathrm{e}^{-\mathbf{A}t}\left[\boldsymbol{\Sigma}(0) - \boldsymbol{\Sigma}_\mathrm{s}\right]\mathrm{e}^{-\mathbf{A}^T t}\right)\mathbf{A}^T \\
&= -\mathbf{A}\boldsymbol{\Sigma}(t) + \mathbf{A}\boldsymbol{\Sigma}_\mathrm{s} - \boldsymbol{\Sigma}(t)\mathbf{A}^T + \boldsymbol{\Sigma}_\mathrm{s}\mathbf{A}^T \\
&\overset{(\mathrm{S12})}{=} -\mathbf{A}\boldsymbol{\Sigma}(t) - \boldsymbol{\Sigma}(t)\mathbf{A}^T + 2\mathbf{D}.
\end{aligned}
\tag{S14}
$$

Choosing $\boldsymbol{\Sigma}(0) = \boldsymbol{\Sigma}_{\mathrm{s},i} = T_i \boldsymbol{\Sigma}_{\mathrm{s},w}/T_w$ yields Eq. (4) in the Letter.

III. GENERALIZED EXCESS FREE ENERGY DURING HEATING AND COOLING

The Kullback-Leibler divergence [Eq. (1) in the Letter] can be computed for two d-dimensional Gaussian densities $P_{1,2}$ with mean zero as $2D_{\mathrm{KL}}(P_1 \| P_2) = -\ln\left(\det\left[\boldsymbol{\Sigma}_1 \boldsymbol{\Sigma}_2^{-1}\right]\right) + \mathrm{tr}\left(\boldsymbol{\Sigma}_1 \boldsymbol{\Sigma}_2^{-1} - \mathbb{1}\right)$ where $\mathbb{1}$ is the d-dimensional unit matrix. Using Eq. (4) in the Letter (i.e. $\boldsymbol{\Sigma}_i^w(t) = \boldsymbol{\Sigma}_{\mathrm{s},w} + \mathrm{e}^{-\mathbf{A}t}\left[\boldsymbol{\Sigma}_{\mathrm{s},i} - \boldsymbol{\Sigma}_{\mathrm{s},w}\right]\mathrm{e}^{-\mathbf{A}^T t}$) with the notations $\mathbf{X}(t) \equiv \mathrm{e}^{-\mathbf{A}t}\boldsymbol{\Sigma}_{\mathrm{s},w}\mathrm{e}^{-\mathbf{A}^T t}\boldsymbol{\Sigma}_{\mathrm{s},w}^{-1}$ and $\delta\tilde{T}_i \equiv T_i/T_w - 1$ we obtain Eq. (5) in the Letter, i.e.

$$
\mathcal{D}_t^i = \frac{1}{2}\delta\tilde{T}_i \,\mathrm{tr}\mathbf{X}(t) - \frac{1}{2}\ln\det\left[\mathbb{1} + \delta\tilde{T}_i \mathbf{X}(t)\right].
\tag{S15}
$$

IV. EFFECTIVE ROTATIONS OPPOSING THE DIRECTION OF DRIFT

In the Letter (see Fig. 2e-f) we state that, and briefly explain why, rotations of the probability density function (quantified via covariance ellipses) during heating emerge in opposite directions. Mathematically opposing rotations can be seen from Eq. (4) in the Letter, $\boldsymbol{\Sigma}_i^w(t) = \boldsymbol{\Sigma}_{\mathrm{s},w} + \mathrm{e}^{-\mathbf{A}t}\left[\boldsymbol{\Sigma}_{\mathrm{s},i} - \boldsymbol{\Sigma}_{\mathrm{s},w}\right]\mathrm{e}^{-\mathbf{A}^T t}$, where $\boldsymbol{\Sigma}_{\mathrm{s},i} - \boldsymbol{\Sigma}_{\mathrm{s},w} = (T_i/T_w - 1)\boldsymbol{\Sigma}_{\mathrm{s},w}$ has opposing signs for $T_c < T_w$ and $T_h > T_w$. However, the physical or phenomenological understanding is more challenging. The most surprising aspect is that rotational motions occur in directions that oppose the rotational driving (e.g., during heating). Since there are no rotational motions in the absence of driving, clockwise rotational driving can in fact lead to counterclockwise (effective) rotations.

First, note that the phenomenon has to be understood on the level of probability density functions and *not* on the level of individual particles' trajectories. In Fig. S1a,b we show that the cloud of particles' positions (representing
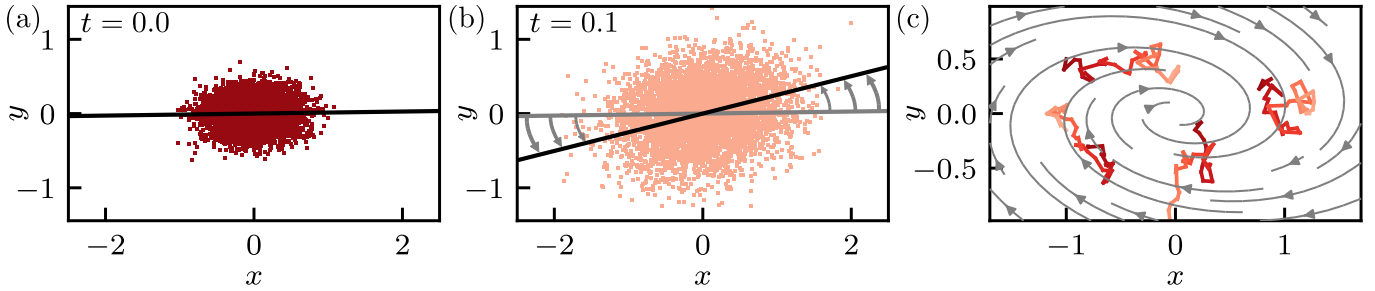
FIG. S1. (a,b) Simulation of 5000 particles' trajectories evolving according to the two-dimensional overdamped Langevin equation $d\mathbf{x}_t = -\mathbf{A}\mathbf{x}_t dt + \sqrt{2}d\mathbf{W}_t$ with $\mathbf{A} = \begin{bmatrix} r_1 & -r_2\omega \\ -r_1\omega & r_2 \end{bmatrix}$ with $r_1 = 1$, $r_2 = 3$, $\omega = 8\omega_c$ and time-step $dt = 0.001$ starting from an initial condition corresponding to $T_c = 0.1$ (in units of T_w). (c) Simulated trajectories of 4 particles in time 0.0 (dark) to 0.1 (bright). Grey streamlines shows $\mathbf{A}(x,y)^T$, i.e., the direction that particles' trajectories follow on average.

the probability density) effectively rotates in the counterclockwise direction while the individual particles on average follow the rotational drift in the clockwise direction, see Fig. S1c.

The emergence of this counterintuitive opposing rotation is explained in Fig. 2f in the Letter. To repeat this, during a Trotterized time-increment the diffusion propagates the initial covariance ellipse to a more circular (less eccentric) one. Next, note that the rotational drift is *not* a perfect circulation, but instead driving along elliptical contour-lines *plus* the driving into the center due to the confining (conservative) potential. This clockwise elliptical rotational driving applied to the ellipse (previously "rounded" during the diffusion Trotter-increment) leads to the counter-clockwise rotation directly by following the streamlines of the drift (see Fig. 2f in the Letter).

To elaborate on these rotations consider Fig. S2. Ellipses in Fig. S2 and those shown below are the covariance ellipses, while ellipses in Fig. S1 and Fig. 2f in the Letter correspond to standard-deviation ellipses (i.e., square roots of covariance ellipses). In Fig. S2a we recall the opposite rotation during heating and cooling. As in Fig. S1 we then focus on the heating, where the initial rotation is in the counterintuitive direction; see Fig. S2b. To illustrate the explanation given in Fig. 2f in the Letter, we show that this rotation similarly emerges if we start in a circular initial condition (see Fig. S2c).

If we instead consider a circular driving with circular steady-state density (see Fig. S2d) all rotations emerge in the (intuitive) clockwise direction, which shows that the elliptical (i.e. non-circular) component of the circular driving is a key factor in this phenomenon.
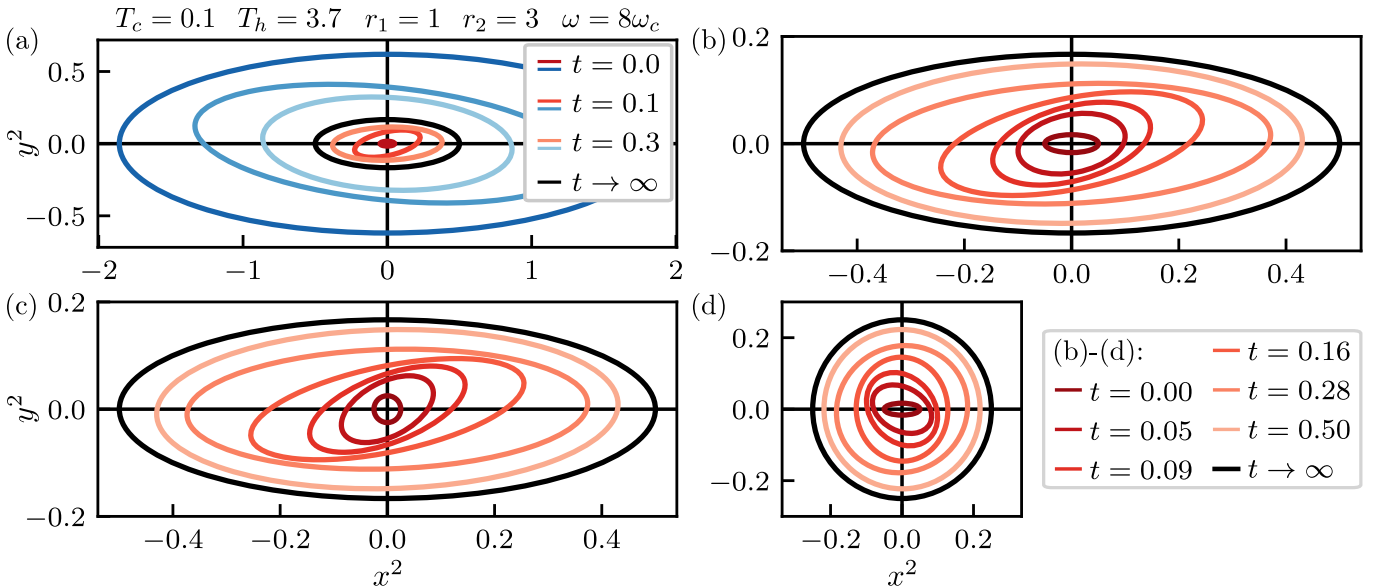
FIG. S2. (a,b) Covariance ellipses from Eq. (S13) for heating and cooling for the process as in Fig. S1 and Fig. 2 in the Letter. (c) As in (b) but with initial condition with $r_1 = r_2 = 2$. (d) As in (b) but with process (but not initial condition) defined with $r_1 = r_2 = 2$.

In Fig. S3 we further illustrate the relation between the direction of rotation and the shape of covariance ellipses. As explained above and in Fig. 2f in the Letter, a more circular (less eccentric) ellipse [sign(3−ratio)=1] leads to a surprising counter-clockwise rotation [sign(angle-change)=1]. The overlap of the curves in Fig. S3c,d corroborates this explanation. Small deviations between the curves emerge since the heuristic explanation only applies to ellipses with angle(t) = 0.
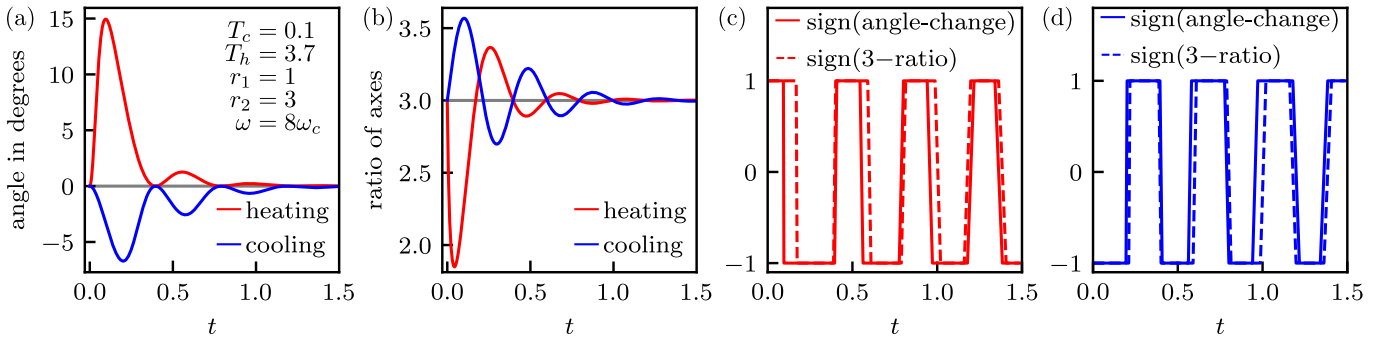
FIG. S3. (a) Same as in 2e in the Letter. (b) Ratio of the axes of the covariance ellipse. Values below 3 reflect more circular (less eccentric) ellipses compared to the initial condition and the steady state. (c,d) Direction of rotation (clockwise rotation is +1) and indicator of shape (±1 means more/less round, i.e., less/more eccentric) for heating (c) and cooling (d).

In Fig. S4 we repeat the presentation of Fig. S3 for a case where the eigenvalues of the drift matrix are real (see Fig. 2d in the Letter for $\omega < \omega_c$). We observe that (opposite) rotational motions also occur for the case of real eigenvalues, which illustrates that (effective) rotational motions do *not only* emerge for complex eigenvalues. A difference with respect to Fig. S3 is that the angles do not cross 0 such that the explanation for the overlaps in Fig. S4c,d only applies at $t = 0$.
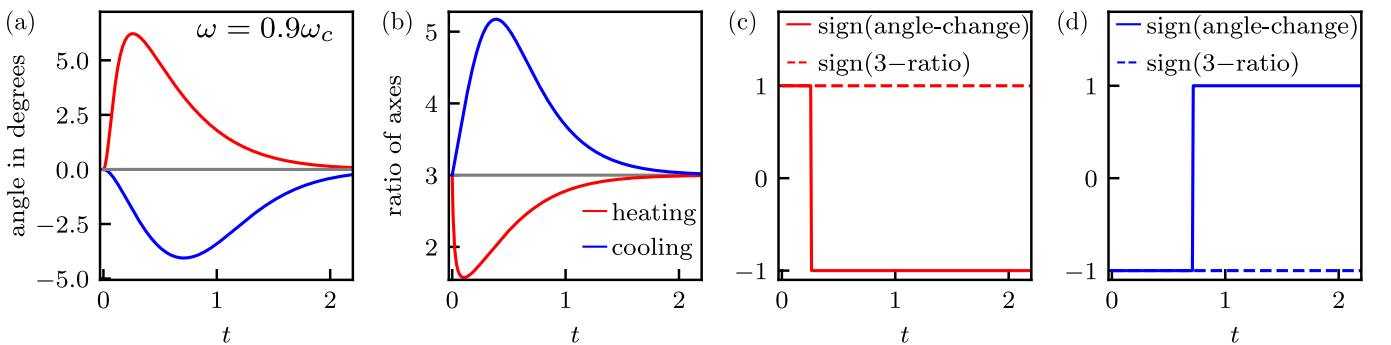
FIG. S4. As in Fig. S3 but for $\omega = 0.9\omega_c$, i.e., eigenvalues of the drift matrix $\mathbf{A}$ are real (see Fig. 2d in the Letter).

Relevance and generality of the observation of counterintuitive rotations

So far we only investigated the origin of the counterintuitive rotations in the two-dimensional example. However, since such counterintuitive rotations already occur in this linear, low-dimensional example, it is to be expected that such motions also occur for more general driven systems. In particular, if two-dimensional subspaces are described by the example above one immediately has this rotation in the subspace of the more general dynamics. Generally, one expects opposite rotations during heating and cooling (and therefore one of the two has to rotate opposite to the driving) due to the difference in sign of $\mathbf{\Sigma}_{\mathrm{s},i} - \mathbf{\Sigma}_{\mathrm{s},w} = (T_i/T_w - 1)\mathbf{\Sigma}_{\mathrm{s},w}$ for $i = h, c$ in Eq. (S13) [Eq. (4) in the Letter] as pointed out above.

The relevance of this observation is twofold. On the one hand, it further emphasizes the asymmetry between heating and cooling, and that the process does *not* pass through locally equilibrated states (i.e., the system *cannot* be described by a time-dependent temperature). On the other hand, it is also relevant for general relaxation phenomena, i.e. beyond thermal relaxation. For example, imagine one observes the part of the relaxation process in Fig. S1a,b for $t \in [0, 0.1]$. If one only observes the apparent counterclockwise rotation of the probability density, one would never

guess that the underlying driving is actually in the clockwise direction. Therefore, awareness of this counterintuitive phenomenon might prove useful to avoid false conclusions; and a deep understanding of this phenomenon helps to arrive at correct conclusions.

V. CONSISTENT COMPARISON OF EQUILIBRIUM AND NON-EQUILIBRIUM STEADY STATES

We here discuss under which circumstances we consider a comparison of equilibrium (EQ) and non-equilibrium steady states (NESS), or of different NESS, to be *consistent*.

In short, we consider a comparison to be consistent if tuning the driving strength does *not* change the steady-state density. Before we explain this in detail, we want to stress that a consistent comparison *is by no means required for the statement of the thermal relaxation asymmetry to be valid*, since this statement is proven for *any* NESS with linear drift in the Letter. Therefore, we were able to chose the physical example of a Rouse chain in a shear flow to illustrate the relaxation asymmetry in Fig. 1 in the Letter (which in fact does *not* represent a consistent comparison). The consistent comparison is, however, necessary for the statement of "accelerated relaxation" since this statement compares the relaxation speed towards an NESS with the relaxation speed in the *corresponding* passive system relaxing into an equilibrium steady state.

In the Letter, we use Eq. (3), i.e. Eq. (S12), to obtain the decomposition $\mathbf{A} = (\mathbf{D}_i + \boldsymbol{\alpha}_i)\boldsymbol{\Sigma}_{\mathrm{s},i}^{-1}$ [Eq. (7) in the Letter] with $\boldsymbol{\alpha}_i^T = -\boldsymbol{\alpha}_i$ for the linear drift matrix $\mathbf{A}$. Note that here $\mathbf{D}_i, \boldsymbol{\alpha}_i, \boldsymbol{\Sigma}_{\mathrm{s},i} \propto T_i$ all increase linearly with temperature but the product $\mathbf{A}$ involving $\boldsymbol{\Sigma}_{\mathrm{s},i}^{-1} \propto T_i^{-1}$ is temperature independent. Any $\mathbf{A}$ from this decomposition fulfills Eq. (3) in the Letter, i.e. Eq. (S12), with the given $\boldsymbol{\Sigma}_{\mathrm{s},i}$, and in turn any $\mathbf{A}$ implying a steady-state covariance $\boldsymbol{\Sigma}_{\mathrm{s},i}$ via Eq. (3) in the Letter can be decomposed with this $\boldsymbol{\Sigma}_{\mathrm{s},i}$ according to $\mathbf{A} = (\mathbf{D}_i + \boldsymbol{\alpha}_i)\boldsymbol{\Sigma}_{\mathrm{s},i}^{-1}$. The advantage of the latter form is that it allows to systematically compare NESS dynamics (or in the special case reversible dynamics) $d\mathbf{x}_t = -\mathbf{A}\mathbf{x}_t dt + \boldsymbol{\sigma} d\mathbf{W}_t$ with different $\mathbf{A}$ that possess different driving strengths but the same steady-state density. This comparison is performed by tuning the parameter $\boldsymbol{\alpha}_i$ (reversible systems are obtained by setting $\boldsymbol{\alpha}_i = \mathbf{0}$) for a given $\boldsymbol{\Sigma}_{\mathrm{s},i}$, which then yields $\mathbf{A}$ via $\mathbf{A} = (\mathbf{D}_i + \boldsymbol{\alpha}_i)\boldsymbol{\Sigma}_{\mathrm{s},i}^{-1}$ [Eq. (7) in the Letter]. We consider such a comparison to be *consistent*, in contrast to a comparison where tuning the irreversible driving alters $\boldsymbol{\Sigma}_{\mathrm{s},i}$ and thus the steady-state density.

An example for a driving that does *not* yield a consistent comparison is the shear flow in Fig. 1 in the Letter and in Eqs. (S1)-(S9). We discuss this comparison in detail now. For simplicity we consider a single particle $N = 1$ in the x-y plane subject to the confining potential and shear flow [see Eqs. (S5)-(S7)] described by the equation of motion $d\mathbf{x}_t = -\mathbf{A}\mathbf{x}_t dt + \sqrt{2}d\mathbf{W}_t$ with drift matrix

$$\mathbf{A} = \begin{bmatrix} \cos(\theta) & -\sin(\theta) \\ \sin(\theta) & \cos(\theta) \end{bmatrix} \begin{bmatrix} r_x & 0 \\ 0 & r_y \end{bmatrix} \begin{bmatrix} \cos(\theta) & \sin(\theta) \\ -\sin(\theta) & \cos(\theta) \end{bmatrix} + \begin{bmatrix} 0 & \omega \\ 0 & 0 \end{bmatrix}. \tag{S16}$$

This drift originates from a (rotated) confining potential with confinement strength quantified by $r_x, r_y > 0$, plus a shear flow of strength ω (both exactly as shown in Fig. 1a in the Letter). The drift without the shear flow $\omega = 0$ is symmetric and therefore gives rise to reversible dynamics with steady-state covariance [see Eq. (3) or (7) in the Letter for $\mathbf{D} = \mathbb{1}$]

$$\boldsymbol{\Sigma}_{\mathrm{s}} = \begin{bmatrix} \cos(\theta) & -\sin(\theta) \\ \sin(\theta) & \cos(\theta) \end{bmatrix} \begin{bmatrix} 1/r_x & 0 \\ 0 & 1/r_y \end{bmatrix} \begin{bmatrix} \cos(\theta) & \sin(\theta) \\ -\sin(\theta) & \cos(\theta) \end{bmatrix}. \tag{S17}$$

The shear flow $\omega \neq 0$ renders the dynamics irreversible. However, since now it is not of the form $\boldsymbol{\alpha}\boldsymbol{\Sigma}_{\mathrm{s}}^{-1}$ with $\boldsymbol{\alpha}^T = -\boldsymbol{\alpha}$ as in Eq. (7) in the Letter, the steady-state covariance for $\omega \neq 0$ will no longer be given by Eq. (S17), i.e. the steady-state Lyapunov equation [see Eq. (3) in the Letter or Eq. (S12)] for $\mathbf{A}$ with $\omega \neq 0$ will give rise to another steady-state different from Eq. (S17) which corresponds to $\omega = 0$. Therefore, comparing systems with different ω will generally not be *consistent* [opposed a comparing systems with different $\boldsymbol{\alpha}_i$ in Eq. (7) in the Letter].

We illustrate this *inconsistent* comparison by three different examples. Choosing the parameters $r_x = 1$, $r_y = 0.1$, $\omega = 3, \theta = -10°$ as in Fig. 1a in the Letter, the eigenvalues of $\mathbf{A}$ are $0.55 \pm 0.51i$, i.e. compared to $\omega = 0$ with eigenvalues $r_{x,y}$ the statement of faster relaxation as quantified in Eq. (8) in the Letter does still hold true, even though the proof does not apply here (see also Fig. 1b in the Letter where the curves with the shear flow decay faster at long times). However, if one instead takes $\omega = 0.5, \theta = 10°$ the eigenvalues of $\mathbf{A}$ are 1.08 and 0.02 i.e. the limiting relaxation is *slower* compared to the reversible system since $0.02 < r_{x,y}$. Thus the statement of faster relaxation does not apply since the effect of the shear flow on the steady state is too large. Even more extreme is the case $\omega = 3, \theta = 10°$ where the eigenvalues are 1.365 and -0.265 where the negative eigenvalue implies that the shear flow destroyed the confining potential in the sense that the resulting drift no longer corresponds to a confined process. *This*

means that this process no longer relaxes into an NESS. This can, of course, not happen for a consistent comparison since changing only $\boldsymbol{\alpha}_i$ in Eq. (7) in the Letter does not change the confinement.

VI. ADIABATIC ENTROPY PRODUCTION

The adiabatic entropy production is the housekeeping heat divided by the reservoir temperature and is given by [4]

$$\dot{S}_a(t) = \int d\mathbf{x} P(\mathbf{x}, t) \mathbf{a}_{\mathrm{irr}}(\mathbf{x})^T \mathbf{D}_i^{-1} \mathbf{a}_{\mathrm{irr}}(\mathbf{x}), \tag{S18}$$

where the irreversible drift in the linear case considered in the Letter reads $\mathbf{a}_{\mathrm{irr}}(\mathbf{x}) = -\mathbf{A}_{\mathrm{irr}}\mathbf{x} = -\boldsymbol{\alpha}_i \boldsymbol{\Sigma}_{\mathrm{s},i}^{-1} \mathbf{x}$. Thus, we see that the adiabatic entropy production term scales linearly with $\boldsymbol{\alpha}_i^T \mathbf{D}_i^{-1} \boldsymbol{\alpha}_i$ as mentioned in the Letter, i.e. it scales quadratically in the driving strength.

VII. LONG-TIME SCALING OF THE KULLBACK-LEIBLER DIVERGENCE

In terms of the eigenvalue λ_1 of $\mathbf{A}$ that has the smallest real part, we know that asymptotically for large t the magnitude of $\mathrm{e}^{-\mathbf{A}t}$ is determined by $\mathrm{e}^{-\Re(\lambda_1)t}$ [there may still be oscillations (see Fig. 2h in the Letter) and if $\mathbf{A}$ is not diagonalizable there may also be terms $t^k \mathrm{e}^{-\Re(\lambda_1)t}$ with $k \in \mathbb{N}$ entering, which nonetheless are dominated by $\mathrm{e}^{-\Re(\lambda_1)t}$ for sufficiently large t]. Note that $\mathrm{e}^{-\mathbf{A}t} \sim \mathrm{e}^{-\Re(\lambda_1)t}$ implies, via Eq. (6) in the Letter, that $\mathbf{X}(t) \sim \mathrm{e}^{-2\Re(\lambda_1)t}$ for $t \to \infty$. Recall Eq. (5) in the Letter, i.e. $2\mathcal{D}_t^i = \mathrm{tr}[\delta \tilde{T}_i \mathbf{X}(t)] - \ln \det[\mathbb{1} + \delta \tilde{T}_i \mathbf{X}(t)]$. Considering $\delta \tilde{T}_i \mathbf{X}(t) = \mathrm{e}^{-2\Re(\lambda_1)t}\mathbf{M}$ for some matrix $\mathbf{M}$ for large enough t and using that around $\mathrm{e}^{-2\Re(\lambda_1)t} \to 0$, we have that $\det[\mathbb{1} + \mathrm{e}^{-2\Re(\lambda_1)t}\mathbf{M}] = 1 + \mathrm{tr}[\mathrm{e}^{-2\Re(\lambda_1)t}\mathbf{M}] + \mathcal{O}[\mathrm{e}^{-4\Re(\lambda_1)t}]$, and we obtain $\mathcal{D}_t^i = \mathcal{O}[\mathrm{e}^{-4\Re(\lambda_1)t}]$ as illustrated in Fig. 2h in the Letter. This confirms that the limiting relaxation speed is dictated by $\Re(\lambda_1)$, i.e. by the smallest real part of eigenvalues of $\mathbf{A}$. In the reversible case we have $\Re(\lambda_1) = \mu_1$ with the notation in the Letter, and $\mu_1 = r_1$ for the example considered in Fig. 2 in the Letter.

Note that we did not formally exclude the case that the order $\mathrm{e}^{-4\Re(\lambda_1)t}$ also vanishes; in this situation we would need to consider even higher orders. It is likely that this case can be generally excluded, however, since no results hinge on the specific scaling, we do not go into more detail here.

VIII. EFFECTIVE STIFFNESS

The effective stiffness $\hat{r}_j(\omega) \equiv -\ln(x_j^t)/2t$ [such that $x_j^t = \mathrm{e}^{-2\hat{r}_j(\omega)t}$] is defined as the stiffness of the confining potential of a reversible system that has the same thermal relaxation properties as the considered system, where x_j^t for $j = 1, \ldots, d$ are the eigenvalues of the matrix $\mathbf{X}(t) \equiv \mathrm{e}^{-\mathbf{A}t}\boldsymbol{\Sigma}_{\mathrm{s},w}\mathrm{e}^{-\mathbf{A}^T t}\boldsymbol{\Sigma}_{\mathrm{s},w}^{-1} = \mathrm{e}^{-\mathbf{A}t}\mathrm{e}^{-\mathbf{A}_{-\alpha}t}$ [see Eqs. (6) and (10) in the Letter]. In Fig. 3b in the Letter we show $\hat{r}_j(\omega)$ for $j = 1, 2$ for the two-dimensional system as shown in Fig. 2 in the Letter with driving strength ω. The eigenvalues $x_{1,2}^t$ at $T_w = 1$ (i.e. T_i are measured in units of T_w) for this example are computed from

$$\mathbf{A} \equiv \begin{bmatrix} r_1 & -r_2\omega \\ r_1\omega & r_2 \end{bmatrix}, \qquad \boldsymbol{\sigma} = \sqrt{2}\mathbb{1}, \qquad \boldsymbol{\Sigma}_{\mathrm{s}} = \begin{bmatrix} 1/r_1 & 0 \\ 0 & 1/r_2 \end{bmatrix},$$

$$M \equiv \sqrt{(r_1 - r_2)^2 - 4r_1 r_2 \omega^2} \in \mathbb{C},$$

$$\exp(-\mathbf{A}t) = \frac{\exp[-(r_1 + r_2)t/2]}{M} \begin{bmatrix} M\cosh\left(\frac{Mt}{2}\right) - |r_1 - r_2|\sinh\left(\frac{Mt}{2}\right) & 2\omega r_2 \sinh\left(\frac{Mt}{2}\right) \\ -2\omega r_1 \sinh\left(\frac{Mt}{2}\right) & M\cosh\left(\frac{Mt}{2}\right) + |r_1 - r_2|\sinh\left(\frac{Mt}{2}\right) \end{bmatrix},$$

$$x_1^t x_2^t = \det[\mathbf{X}(t)] = \exp[-2(r_1 + r_2)t],$$

$$x_1^t + x_2^t = \mathrm{tr}[\mathbf{X}(t)] = 2\exp[-(r_1 + r_2)t]\left[1 + 2\frac{(r_1 - r_2)^2}{M^2}\sinh^2\left(\frac{Mt}{2}\right)\right]$$

$$x_{1,2}^t = \frac{\mathrm{tr}(\mathbf{X}(t))}{2} \pm \sqrt{\frac{\mathrm{tr}^2(\mathbf{X}(t))}{4} - \det(\mathbf{X}(t))}. \tag{S19}$$

IX. LOG-NORM INEQUALITY

In the Letter we use the log-norm inequality $||\exp(\mathbf{M}t)|| \leq \exp[\mu(\mathbf{M})t]$ [5] where the log norm is defined via the matrix norm $||\mathbf{M}|| \equiv \sup_{\mathbf{v} \in \mathbb{R}^d \setminus \mathbf{0}} ||\mathbf{M}\mathbf{v}||_2/||\mathbf{v}||_2$ (also known as operator norm) where $||\mathbf{v}||_2 = \sqrt{\mathbf{v}^T\mathbf{v}}$ as

$$\mu(\mathbf{M}) \equiv \lim_{h \to 0^+} \frac{||\mathbb{1} + h\mathbf{M}|| - 1}{h}. \tag{S20}$$

Writing the matrix norm $||\mathbf{M}||$ in the form $||\mathbf{M}\mathbf{v}||_2/||\mathbf{v}||_2 = \sqrt{\mathbf{v}^T\mathbf{M}^T\mathbf{M}\mathbf{v}/\mathbf{v}^T\mathbf{v}}$ one sees that $||\mathbf{M}||$ is given by the square root of the largest eigenvalue of the symmetric matrix $\mathbf{M}^T\mathbf{M}$. Splitting $\mathbf{M} = \mathbf{M}_s + \mathbf{M}_a$ with $\mathbf{M}_s \equiv (\mathbf{M} + \mathbf{M}^T)/2 = \mathbf{M}_s^T$ and $\mathbf{M}_a \equiv (\mathbf{M} - \mathbf{M}^T)/2 = -\mathbf{M}_a^T$ we find that

$$(\mathbb{1} + h\mathbf{M})^T(\mathbb{1} + h\mathbf{M}) = (\mathbb{1} + h\mathbf{M}_s - h\mathbf{M}_a)(\mathbb{1} + h\mathbf{M}_s + h\mathbf{M}_a) = 1 + 2h\mathbf{M}_s + \mathcal{O}(h^2)$$
$$= (\mathbb{1} + h\mathbf{M}_s)^T(\mathbb{1} + h\mathbf{M}_s) + \mathcal{O}(h^2). \tag{S21}$$

This implies that $||\mathbb{1} + h\mathbf{M}|| = ||\mathbb{1} + h\mathbf{M}_s||$ and via Eq. (S20) that the log norm is solely determined by the symmetric part $\mu(\mathbf{M}) = \mu(\mathbf{M}_s)$. Intuitively this states that asymmetric contributions (which account for rotations after exponentiation) do not enter the absolute value in the exponential bound $||\exp(\mathbf{M}t)|| \leq \exp[\mu(\mathbf{M})t]$, which makes the log norm very useful for our theory.

From this insight we immediately compute the result used in the Letter, i.e. we use that $-\boldsymbol{\beta}\mathbf{D}_w\boldsymbol{\beta}$ with eigenvalues $-\mu_1 > -\mu_2 > \ldots$ is the symmetric part of $-\boldsymbol{\beta}\mathbf{A}\boldsymbol{\beta}^{-1}$ to obtain

$$\mu(-\widetilde{\mathbf{A}}) \equiv \mu(-\boldsymbol{\beta}\mathbf{A}\boldsymbol{\beta}^{-1}) = \mu(-\boldsymbol{\beta}\mathbf{D}_w\boldsymbol{\beta}) = -\mu_1. \tag{S22}$$

---

[1] R. R. Cheng, A. T. Hawk, and D. E. Makarov, J. Chem. Phys. **138**, 074112 (2013).

[2] N. Ikeda and S. Watanabe, *Stochastic Differential Equations and Diffusion Processes*, 1st ed. (North Holland, 1981) eBook ISBN: 9780080960128.

[3] C. W. Gardiner, *Handbook of Stochastic Methods for Physics, Chemistry, and the Natural Sciences* (Springer-Verlag, Berlin New York, 1985).

[4] C. Van den Broeck and M. Esposito, Phys. Rev. E **82**, 011144 (2010).

[5] G. Dahlquist, *Stability and Error Bounds in the Numerical Integration of Ordinary Differential Equations* (Almqvist & Wiksell, Uppsala, Sweden, 1958).